

# MULTI-OBJECTIVE INDUSTRIAL OPTIMIZATION OF HIGH-SPEED HELICOPTER MAIN ROTOR BLADES WITH DYNAMICALLY-ADAPTED STRUCTURAL PROPERTIES

D. Desvigne, R. Coisson, B.R. Michel, A. Thomas & J.P. Pinacho  
Airbus Helicopters S.A.S.  
Marseille-Provence International Airport, F-13725 Marignane cedex, France

E. Roca León  
Altran Technologies  
4 avenue Didier Daurat, F-31700 Blagnac, France

## Abstract

A multidisciplinary multi-objective optimization tool chain developed for designing main-rotor blades of high-speed helicopters is presented. Objectives focus on the dynamic loads in high-speed level flight, along with rotor power in hover. The tool chain relies on a genetic algorithm coupled to loads and performance simulation tools. In order to fulfill potentially strong industrial constraints, low-cost models are used in the comprehensive rotor simulation code HOST.

Dynamic control loads may become critical in high speed and accurately representing both inertial and elastic responses of the blade to aerodynamic excitations is essential in the blade-design process. A new methodology is proposed in this work for the modelling of the blade structural properties. The strategy adopted is as follows: the design space is first sampled with a fixed number of donor-blade designs which cover most of the foreseen realistic planforms. The internal structure of each donor blade is tailored so that the blade eigenfrequencies placement is optimal with respect to the rotor harmonics, together with a mitigation of the blade-to-cabin modal transmissibility. Then, for each design candidate in the optimization process, a relevant donor blade is selected amongst the donor pool based on geometric similarities. The candidate structural properties are finally obtained by correcting the donor structural description with empirical functions based on the geometric discrepancies, assuming a similar structural technology.

Twist, chord, and offset spanwise distributions are parameterized with Bézier curves and an optimization procedure is conducted so as to minimize the required power for hovering as well as to minimize the dynamic control loads in high-speed cruise conditions. A Pareto optimal solution is chosen and a more detailed analysis is achieved using higher-fidelity tools.

The inclusion of the automatic structural update provides more realistic blade designs. The analysis of the updated structural properties indicates that the hypothesis assuming that the donor and the candidate blade have very similar eigenmodes is not entirely verified. Nevertheless, the method yields promising candidates and demonstrates the challenge of integrating the blade internal properties into the global industrial design process.

## 1. INTRODUCTION

The industrial process for the design of main rotor blades implies finding the best compromise for several flight conditions which are often antagonistic in nature, such as hover and forward flight. Multi-disciplinary issues must be considered in order to meet performance, loads and acoustics goals. Rotor designs suitable for high-speed flight must take into account even stricter constraints as challenges emerge with the increase of the advance ratio, such as the amplified dynamic control loads which can reduce significantly the lifetime of rotor-head components. As a consequence of these design challenges, blade optimization has been the focus of numerous studies in the last decades [11][15].

Numerous studies have been focused on the blade structural optimization with the goal to reduce hub loads using structural variables [13] and a reduced number of shape variables [12]. These approaches use simplified aerodynamics in order to solve the aeroelastic problem. Multi-objective optimizations aiming at improving rotor performance and/or acoustics make increasingly use of Computational Fluid Dynamics (CFD) [16][17][20][28][29][34]. However, the computational costs

remain still too high to consider full CFD global optimizations in an industrial context. The adjoint approach in its steady [10] and unsteady formulations [7][22] has been successfully applied to local optimizations allowing the computation of gradients at a small cost. The computational cost of high-fidelity CFD simulations in global optimization problems can be somewhat alleviated with the use of surrogate models [17] and/or multi-fidelity approaches [4][8][20][28][34] combining information from low and high simulation tools. The use of coupled CFD/CSD remains challenging, as the fluid-structure interactions are non-negligible. Blade structural properties are frequently considered frozen through optimization studies, which can lead to unrealistic designs [29]. Some recent studies have tackled the fast update of shape variations [32]. More recently, parametric studies were performed including structural data updates and structural constraints [21]. Structural data updates were proposed as well by ONERA [3] without additional structural constraints in a low-fidelity optimization loop and soon afterwards high-fidelity evaluations via co-kriging surrogate models were added to the existing framework [4].

This work addresses this issue from an industrial perspective: fully coupled CSD/CFD computations in the

frame of a pre-design optimization process remain prohibitively expensive. Additionally, in order to produce realistic results, the workflow should include an update of blade structural properties for each design. A low-fidelity approach is proposed so as to include this structural update in the design loop for fast global exploration of blade designs.

## 2. THE HIGH-SPEED HYBRID HELICOPTER CONCEPT (H<sup>3</sup>)

### 2.1. The high-speed challenge for helicopters

For conventional helicopters, the inherent asymmetric nature of the flow over the main rotor gives rise to a number of aerodynamic problems, which generally appear in four areas [18] as illustrated in Figure 1:

- i. The blade tip on the advancing side may enter into transonic flow regimes with the associated generation of shock waves, wave drag and shock-induced flow separations so that Mach tuck may occur and more power is required to drive the rotor;
- ii. On the retreating side, the local velocity is low so that the blade has to operate at high angles of attack (AoA) to preserve the lift generation. Blade stall may occur if the AoA values become too large, resulting in a loss of thrust production as well as the generation of unsteady airloads which can limit the rotorcraft forward-flight capability accordingly;
- iii. A reverse-flow region appears at the retreating side, in which the blade is attacked by the trailing edge. This entails a significant production of profile drag, negative lift and nose-up pitching moment. The greater the rotorcraft speed, the wider the reverse-flow region;
- iv. An asymmetry in the lift distribution in forward flight is observed. Lift is principally produced in the front and aft regions of the rotor disk. Considering the very different flow conditions between advancing and retreating sides, a special care has to be taken to ensure the rotorcraft balance along the roll axis.

The advance ratio  $\mu$  is introduced in what follows. It is defined as the ratio between the rotorcraft translation speed  $U$  to the blade-tip rotation speed  $\Omega R$ , where  $\Omega$  is the rotor angular velocity and  $R$  the rotor radius. The aerodynamic issues previously reported are expected to worsen for high advance ratios, because of the increase of the Mach number at the advancing blade tip, the wider reverse-flow region, and the loss of dynamic pressure at the retreating side where dynamic stall is more likely to occur. Therefore, to allow an extension of the helicopter flight envelope to high-speed level flights, the following requirements need to be addressed respectively for each of the problems previously listed:

- i. The rotor angular velocity must be reduced;
- ii. The blade pitch angle at the retreating blade must be reduced;
- iii. The blade root design including airfoil selection must be adapted to an attack from both the leading and trailing edges;
- iv. The lift generation must be shared with other lifting components.

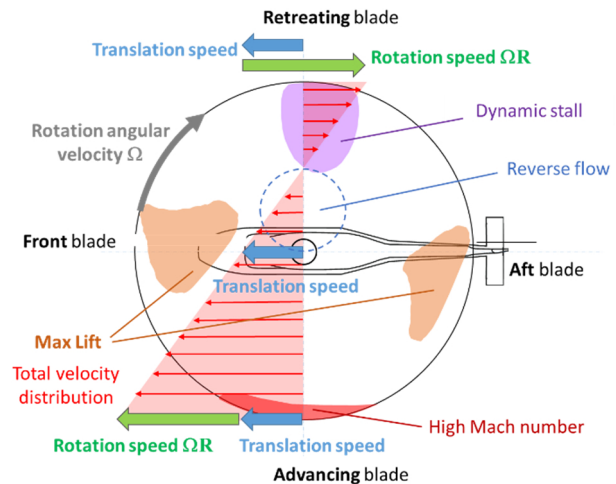


Figure 1 – Overview of typical aerodynamic problem areas occurring on a conventional helicopter rotor in forward flight

### 2.2. The compound helicopter concept

A solution to those needs is proposed throughout the compound helicopter concept, which consists in the addition of auxiliary propulsion systems to reduce high pitch angles of the blade at the retreating side, and the addition of a second rotor or wings to share the lift generation. The compounding of a helicopter is not a new idea. Several flight tests programs that investigated the compound helicopter configurations in the 1960's showed the numerous challenges to overcome before achieving a production vehicle [2][19][24].

#### 2.2.1. X<sup>3</sup>

A major and recent demonstrator of this concept is the X<sup>3</sup> compound helicopter of Eurocopter [19], which combines a conventional helicopter main rotor with two lateral rotors at the tip of a wing. The two lateral rotors provide thrust in level flight, and generate anti-torque and yaw control. This experimental High-Speed Hybrid Helicopter (H<sup>3</sup>) demonstrator was intensively tested in the 2010's for numerous flight conditions, and an extensive test database was produced. It was demonstrated that three possible rotorcraft trims are possible in forward flight depending on the thrust of the lateral rotors: a trim with a propulsive rotor mode like for conventional helicopters, a trim with a neutral rotor mode, and a trim in autogiro rotor mode [23]. In the high-speed cruise nominal mode, the trimmed rotor shows a neutral flat position so that 100% of the propulsion is ensured by the two lateral rotors and up to 50% of the lift generation is transferred to the wings, as shown in Figure 2.

This allows to significantly unload the main rotor and slow down its angular velocity. The high-speed capabilities of the H<sup>3</sup> concept and the validation of the aerodynamic configuration was proven with the achievement of an unofficial record at 255kt in level flight [23].

Nevertheless, the flight tests in level flight revealed that the magnitude of the peak-to-peak dynamic control loads rapidly increases with the advance ratio [26]. This was also the typical trend reported by Sikorsky for the pioneer NH-3A [30] and RSRA [2] hybrid helicopters, as illustrated in Figure 3.

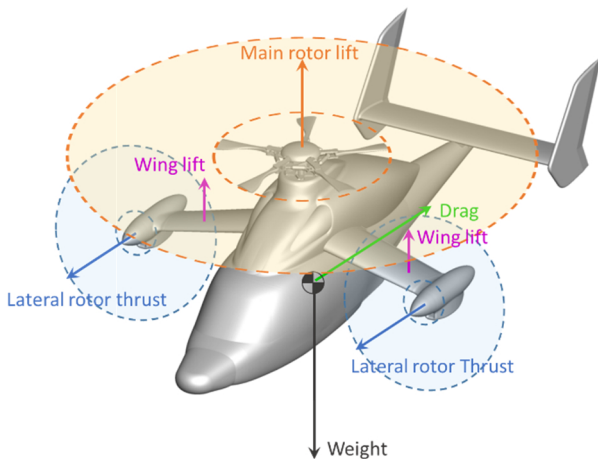


Figure 2 – Compound helicopter trim with a neutral rotor mode in high-speed level flight

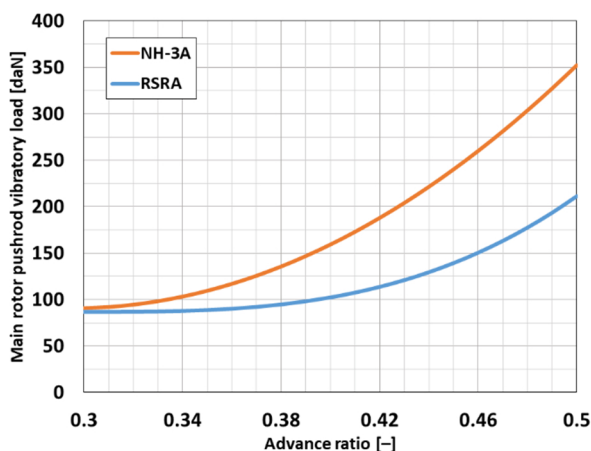


Figure 3 – Typical half peak-to-peak vibratory control loads w.r.t. advance ratio for SRSA & NH-3A compound helicopters, from [2]

The impact of such dynamic loads may be strong on some rotor-head components e.g. the control pushrods. Indeed, heavy unsteady airloads may reduce their lifetime and induce a flight-envelope limitation accordingly.

#### 1.1.1. RACER

The Rapid and Cost-Effective Rotorcraft (RACER) project is the new generation of the H<sup>3</sup> demonstrator, developed as part of the Clean Sky 2 European research programme upon the success of the X<sup>3</sup> demonstrator, as illustrated in Figure 4. RACER is aimed at bringing the H<sup>3</sup> concept closer to an operational design as well as demonstrating its suitability for a wide spectrum of missions where increased speed and efficiency bring significant added value: health & emergency medical services (HEMS), search and rescue (SAR) operations, as well as parapublic services and private & business aviation [1]. The targeted cruise speed ( $V_H$ ) is 220kt and up to 260kt for the dive speed ( $V_D$ ).

Amongst all the actions undertaken to meet those objectives, reducing the operational maintenance burden is a key challenge. For the rotor assembly, this means to keep under control the dynamic loads exerted onto the pushrods in high-speed level flight to preserve their lifetime. The problem is tackled in the Rotor hAutes PerformAnCes urbainEs (RAPACE) research project, supported by the Direction Générale de l'Aviation Civile (DGAC). The

RAPACE project is intended to upgrade the rotor assembly of typical medium-class weight helicopters, including the five blades equipping the RACER demonstrator, with a technology more suitable to the high-speed level flight without penalizing the hover capabilities of the rotorcraft.



Figure 4 – The RACER demonstrator, from [1]

### 3. THE H3 BLADE OPTIMIZATION PROBLEM

In this section, the major RAPACE objectives are presented following a ranking based on priorities. Because the success for any design depends on the choice of points of sizing, a special care has been taken for the selection of optimization objectives and associated flight conditions.

#### 3.1. Mitigate dynamic loads in high-speed level flight

Dynamic loads in high-speed concentrate the largest part of the effort. For the reasons explained in section 2, the priority-one objective is to bring the dynamic control loads experienced in level flight at 220kt at a level below or similar to the one experienced with conventional helicopters in cruise. The peak-to-peak dynamic loads over a rotor revolution is thus proposed to be minimized. The objective is not to exceed the peak-to-peak dynamic loads of medium-class weight helicopters in a nominal level flight at 150kt. This should ensure adequate lifetime for all the critical rotor-head components in high-speed cruise for RACER. The H175 rotor database was used as reference.

#### 3.2. Preserve hover and low-speed performance

Helicopter transport capability is often limited by the performance at takeoff, in particular from restricted areas for which a vertical maneuver is required. Since this leads to a payload reduction, considerable care must be taken in hover flight which is key for vertical takeoff. Performance is strongly impacted by the external conditions (pressure altitude, temperature), due to required power and available power variations. Nevertheless, because of practical constraints (planning and budget) and to avoid a tedious and too complex process, an exhaustive optimization of the power consumed by the main rotor cannot be envisaged and a single reference condition (SL, ISA) has been considered. Once the optimization performed, this does not preclude a global performance assessment of the obtained blades: an air density / rotor angular velocity reduction allows to estimate the power consumed by the main rotor in the entire takeoff domain.

Low speed performance is also a major challenge since the way required power decreases with speed directly impacts

the height loss in case of a continued takeoff after an engine failure and therefore also the margins with respect to ground level and obstacles. For the reasons mentioned above, this case has not been considered as an optimization criterion.

### 3.3. Mitigate the acoustic footprint

Acoustics is another key driver in new Airbus Helicopters developments. Former noise certifications, as well as research projects, show continuous effort in lowering the environmental footprint of Airbus Helicopters fleet, either through design improvements or through the definition and the implementation of low-noise procedures. A special care was thus taken to acoustics during the investigations.

An acoustic target of -3 EPndB is ambitioned in the RAPACE Project. However, the inclusion of a fast-and-robust acoustic evaluator in the optimization tool chain remains challenging. The acoustic objective has consequently been discarded during the pre-design optimization presented in this work. Acoustics has been treated separately, using state-of-the-art methodology, based on the use of mid- and high-fidelity computation tools.

## 4. DESCRIPTION OF THE OPTIMIZATION TOOL CHAIN

### 4.1. Overview of the optimization approach

In this section, an overview of the developed optimization tool chain is given. The global structure of the tool chain is presented in Figure 6. It is articulated around four main modules, which include:

- An optimizer algorithm
- A blade designer
- A flow solver
- An analysis module

Dedicated Python control scripts allow the data exchange between the different modules.

#### 4.1.1. Optimizer

The optimizer module plays the central role of the tool chain. The selected search heuristic is based on a Multi-Objective Genetic Algorithm (MOGA). This kind of algorithm has been preferred because it demonstrates several advantages that more classical optimization techniques such as gradient-based descent-type methods may not offer [14]:

- Potentially demanding evaluations of gradients or auxiliary functions are not needed;
- A wide set of parameters is manageable without an increase of the algorithm complexity;
- The optimum solution is not limited to a single point; a family of optima is provided out of the multi-objective optimization process;
- The solutions do not depend on the initial guess and the convergence is global.

Genetic algorithms have proven their efficiency in tackling complex problems in non-convex design spaces [9][14].

The NSGA-II algorithm [9] has been embedded in the tool chain accordingly. The general strategy consists in mimicking the mechanics of natural selection. Candidates are fully represented by a set of parameters which play the

role of genes. The algorithm then relies on three elementary operations illustrated in Figure 5:

- Reproduction, which reproduces the Darwin principle of “survival of the fittest”: candidates with the higher fitness function are more likely to be bred into the next generation. During the reproduction procedure, fittest candidates are randomly mated;
- Cross-over, which manages the way two selected candidates are mated. The site for the genome exchange is usually randomly chosen;
- Mutation, which randomly alters a gene with a low probability. It prevents the algorithm from losing potentially power and from being stuck around local optima.

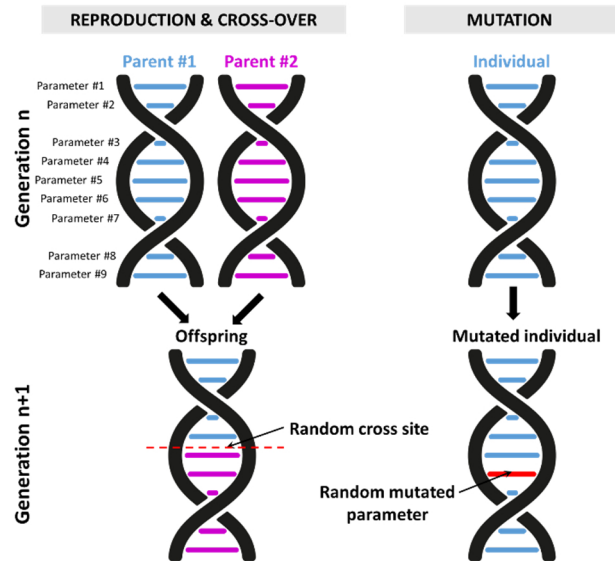


Figure 5 – Illustration of the three operations that drive genetic algorithms: reproduction, cross-over and mutation

The use of MOGA algorithms in the frame of blade design is not new, as it has already been implemented for blade planform generation [20] or airfoil optimization [27].

#### 4.1.2. Blade designer

The NSGA-II algorithm is able to provide randomly-generated parameters in a mathematical hypercube design space. If the geometric design space is not a hypercube, constraints ought to be added as inputs of the optimizer so as to guarantee the geometric consistency of the generated candidates with respect to the geometric design space. In some cases, the determination of constraints may become rapidly complex and non-analytical. This is why the inclusion of a preliminary module out of the candidate generation has been preferred as detailed in section 4.5.

The blade designer consists in three modules managing the generation of a blade geometry given a set of parameters.

The first module is a blade shape processor. Its role is to convert a genetic description of the blade candidates, namely files containing a list of parameters, into a format readable by the flow solver. It can be a CAD geometry which has been meshed or a file containing a tabulated description of the chord, thickness, twist, sweep, anhedral laws and the associated airfoil distribution. In the current implementation of the tool chain, the latter format is retained because it fits the input interface of the selected flow solver.

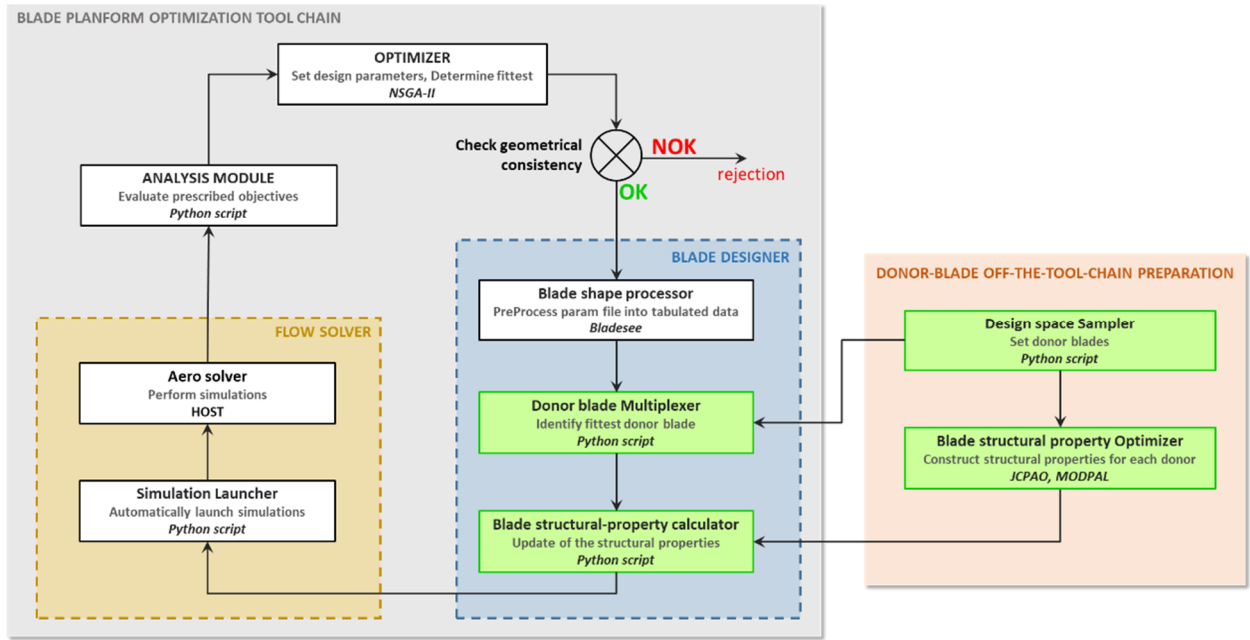


**Figure 6 – Overview of the developed optimization tool chain. The new process tackling the blade internal property adaptation is emphasized with green boxes; the tools employed are reported in italic**

The two other modules deal with the dynamic adaptation of the blade structural properties with geometric changes. They are comprehensively described in section 5.

#### 4.1.3. Flow solver

The selection of the flow solver drives the fidelity (and the associated costs) of the complete optimization procedure. The aerodynamic flow developing around the blade may be assessed directly by computations or it may be modelled. In addition, to offer reliable results, the population constituting a generation and the number of generations must be sufficiently large. As a consequence, the number of candidates to evaluate may become overwhelming. Thus, the use of a Navier-Stokes CFD code in standalone mode or nested in a more complex aeromechanic coupling is too demanding and likely not adapted to an industrial first exploration of potential promising designs.

This is why a faster approach has been preferred, and the Airbus Helicopters' in-house comprehensive rotor simulation code HOST [5] has been selected. The HOST code allows to trim the rotorcraft based on a 2D Blade Element Theory (BET) modal approach. One major difficulty of the BET approach is the proper finding of the induced inflow angle, which is required to compute the sectional angle of attack. This is achieved by resorting to a finite-state inflow model (FISUW) [25]. In the FISUW model, the induced velocity is split into two parts: Legendre polynomials are used for the radial induced velocity distribution, and Fourier series describe the azimuth contribution. A total of 5 harmonics (equal to the number of blades) and 5<sup>th</sup> order radial polynomials were considered in this work. The inflow velocity is determined by the forces on the blade, which are given from look-up tables. An iterative procedure is then applied to find an equilibrium between aerodynamic forces and the inflow velocities.

#### 4.1.4. Analysis module

The analysis module evaluates the optimization objectives for all the candidates. If the objective functions are not direct

outputs of the flow solver, it also must include a routine to extract relevant data from the flow-solver outputs, from which the objectives can be assessed. The objective evaluations are then fed back to the NSGA-II algorithm, and a ranking of the candidates is achieved. This ranking serves as a basis for computing candidate reproduction probabilities.

## 4.2. Blade planform parameterization

In order to limit the parameters to a reasonable number, the airfoil collection and distribution along the blade span are kept very similar to a last-generation rotor blade, with only slight adjustments. The radial location of the first airfoil station  $R_0$  as well as the station corresponding to the start of the blade-tip region  $R_{tip} = 0.945 R$  are also similar. The anhedral distribution is set to 0 all along the blade span.

The blade-planform parameterization is then selected to enable a smooth representation of the chord-, twist- and offset laws along the range  $[R_0, R_{tip}]$  with only a small number of parameters. To this goal, piecewise linear-to-cubic Bézier curves are used. Bézier curves  $B$  are defined from a set of control points  $(P_i)_{i=0..n}$ , where the integer  $n$  represents the degree of the curve, as:

$$(1) \quad B(t) = \sum_{i=0}^n b_{i,n}(t) P_i$$

with  $(P_i)_{i=0..n}$  being the control-point coordinates and  $t$  a parameter sweeping the range  $[0,1]$ . The quantities  $b_{i,n}$  are the Bernstein polynomials of degree  $n$  defined as:

$$(2) \quad b_{i,n}(t) = \binom{n}{i} t^i (1-t)^{n-i}$$

The blade-planform modularity is composed of 21 degrees of freedom.

#### 4.2.1. Chord law

The chord law  $c(r)$  is parameterized by two cubic Bézier curves, as illustrated in Figure 7. The chord values at the Bézier edge points are all degrees of freedom. The two

inner points implemented at the two curves allow a control of the continuity respectively at the junction with the blade root and at the blade-tip region. A flat tangency is imposed at the first airfoil section to guarantee a smooth continuity with the blade root. The two Bézier curves are connected together with a first-order continuity by imposing a flat tangency.

A normalization has been applied for the inner control-point coordinates so as to keep them inside the rectangle defined by the Bézier edge points. As an example, the non-dimensional coordinates of the inner point  $P_{2,2}$  controlling the continuity with the blade-tip region are respectively for the radial and chord coordinate:

$$(3) \quad kP_{2,2r} = \frac{r_{P_{2,2}} - R_1}{R_{tip} - R_1} \quad (4) \quad kP_{2,2c} = \frac{c_{P_{2,2}} - c_1}{c_{tip} - c_1}$$

where  $r_{P_{2,2}}$  and  $c_{P_{2,2}}$  are the radial location and the chord value at point  $P_{2,2}$ .

Those non-dimensional parameters are the ones considered in the optimization procedure for the inner control points. A total of 9 parameters are needed to represent the chord law.

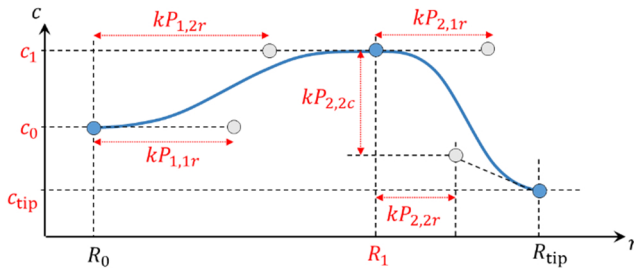


Figure 7 – Parameterization of the chord law; Bézier-curve edge points and inner points are highlighted in blue and grey respectively; Free parameters are emphasized in red

#### 4.2.2. Offset law

The offset law  $\Lambda(r)$  provides a spanwise description of the blade leading-edge location along the chord axis with respect to the pitch axis. An offset of 25% represents a quarter-chord point placed on the pitch axis. As for the chord law, the offset law is parameterized with two cubic Bézier curves, and the same continuity constraints have been considered, as it appears in Figure 8. For the sake of consistency, the control points  $R_1$  and  $P_{i,j}$  have been changed to  $S_1$  and  $Q_{i,j}$  because those are naturally independent from the control points representing the chord law.

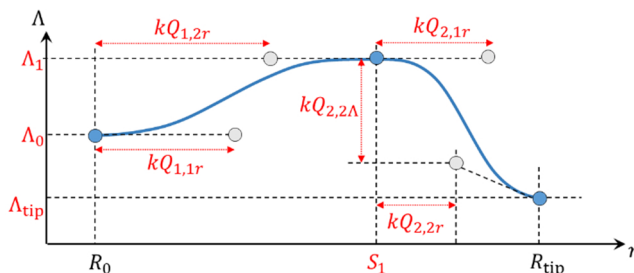


Figure 8 – Parameterization of the offset law; Bézier-curve edge points and inner points are highlighted in blue and grey respectively; Free parameters are emphasized in red

#### 4.2.3. Aerodynamic twist law

A more simple parameterization resorting to three parameters only has been used to represent the blade aerodynamic twist law  $\theta(r)$ . Three piecewise linear twist gradients have been considered between the radial stations  $R_0$ ,  $0.7R$ ,  $0.9R$  and  $R$ , as shown in Figure 9. A zero aerodynamic twist is imposed at  $0.7R$ .

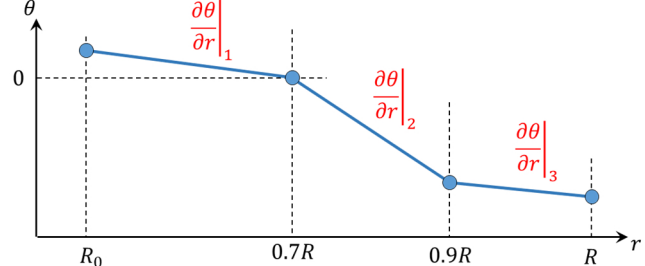


Figure 9 – Parameterization of the aerodynamic twist law; Free parameters are emphasized in red

#### 4.3. Design constraints

For all the candidates, a common tip geometry has been implemented within the radial range  $[R_{tip}, R]$  so as to isolate the contribution of the inner-blade planform only. The adopted geometry of the blade-tip region is based on the parabolic ONERA SPP8 tip design [33]. A slight adaptation has been required to guarantee a first-order continuity of the tip with the blade inner region.

In order to allow a comparison of the different blade candidates in terms of loads and performance, the blade mean aerodynamic chord (MAC) has to be constant for all the candidates. The MAC is defined by:

$$(5) \quad MAC = \frac{\int_{R_0}^R r^2 c(r) dr}{\int_{R_0}^R r^2 dr}$$

Implementing this constraint directly into the optimizer would have required the tedious operation of reformulating analytically equation (5) in terms of the Bézier parameters representing the chord law. The resulting constraint shows a complex form which is not easily manageable by the NSGA-II algorithm. A rescale of the chord law out of the optimizer has been preferred for the sake of simplicity. The MAC is constrained to a constant value.

#### 4.4. Geometric design space

The mathematical design space is obviously a hypercube with 21 dimensions. In terms of geometric space, this corresponds to a 3D space whose axes are respectively the chord-, the offset- and the twist-law representations. The optimum candidates are searched into a polygonal volume represented in Figure 10 along each axis. This polygon has been defined from engineering experience and technological feasibility.

#### 4.5. Candidate consistency check

Parametric non-linear curves are used in the definition of the geometric laws for each radial station. As a consequence, even if boundaries are applied to the Bézier outer points, there is no guarantee that the whole curve will remain into the geometric design space. Only piecewise linear parameterizations would ensure this property without special care. For this reason, an additional check is needed

to guarantee the consistency between the geometric boundaries and the mathematical boundaries.

The geometric laws of each candidate (chord, offset and twist) are thus superposed onto their respective geometric boundary polygon and discretized in upwards of 200 segments. For each point of the discretized curve a check is performed in order to determine if the point lies into the polygon. If all points lie within the boundaries the candidate is deemed valid. Otherwise the candidate is discarded and a penalty value for each of the objective functions is returned to the optimizer in order to discourage further exploration of similar designs.

## 5. MODULES MANAGING THE DYNAMIC ADAPTATION OF THE BLADE STRUCTURAL PROPERTIES

The optimization of the blade planform is based on performance and loads analyses. Such analyses require an elastic blade model, which needs the description of the blade structural properties: stiffness (bending and torsion), inertial and centering (neutral axis, mass centering) properties.

The global strategy adopted to dynamically set the blade structural properties relies on the adaptation of existing blade structures based on geometric discrepancies. The modules dealing with this task can be split into two families, as it appears in Figure 6:

- Modules which are outside the optimization loop. Those are needed to prepare a small pool of blades with tailored internal properties prior to the execution of the optimization procedure;
- Modules which are inside the optimization loop. Those deal with the adaptation of the blade internal properties for all the candidates from the pool of "donor" blades.

### 5.1. Modules outside the optimization loop

#### 5.1.1. Sampling the design space

The goal of this step is to generate a sample of blade planforms, for which a tailoring of the blade internal

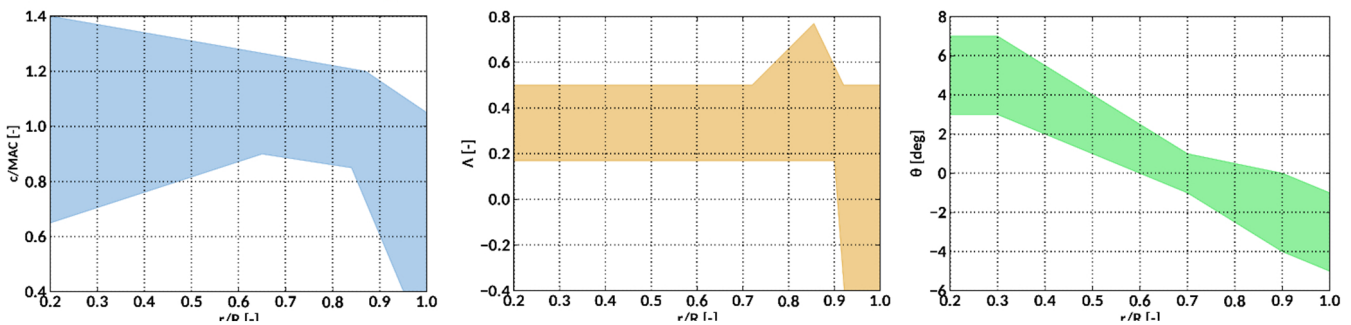


Figure 10 – Overview of the geometric design space (colored polygon); Left : chord; Center: offset; Right : aerodynamic twist

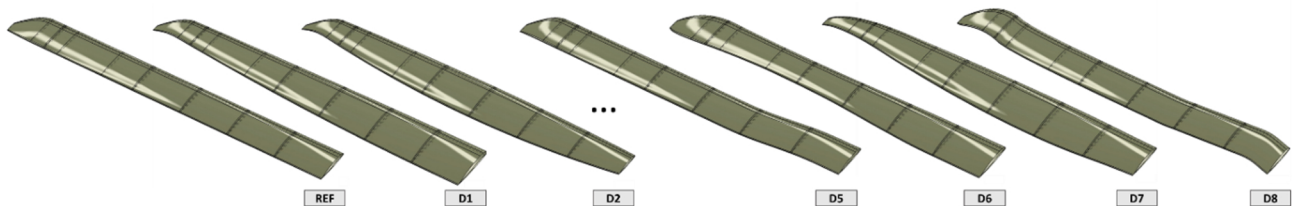


Figure 11 – Overview of the 9-element pool of donor blades

properties is performed. Those planforms will be used to update candidate internal properties in the optimization loop.

The blade is split into three equally distributed parts: the inner, the central and the outer part. In each of those parts, we define three possible states for the chord: small, medium or large. In the same time, the offset may be forward, neutral or backward. The influence of the twist is assumed to be small on the internal properties and is neglected in the design-space sampling procedure. All the combinations of chord-and-offset states define a 27x27 matrix. The number of possible states for the chord may be reduced to 7 because the constraint related to the MAC cannot be fulfilled if the chord is for instance small or large at all the three blade parts. For the offset, the number of states is reduced to 5 because many combinations are known not to be suitable for the problem, e.g. a forward offset all along the blade, or for manufacturing.

The reduced 7x5 matrix is then sampled resorting on the selection of 9 different blade planforms as illustrated in Figure 11 to constitute a pool of donor blades. This pool includes a straight blade for reference.

#### 5.1.2. Tailoring the donor-blade internal properties

Once the set of donor-blade planforms has been defined, their internal structure must be chosen so that the acoustic footprint is minimized, the vibrations in the cabin are as low as possible and the hub and pitch link loads are set to the minimum. The tools currently available do not allow correct predictions of the vibrations in the cabin of a rotorcraft for a given rotor and structure definition. Indeed, there are still shortcomings in the finite-element modelling of a structure and as of today the properties of the structure modes require retuning above 20Hz. Hence, a direct link between the blade design and the cabin vibrations cannot be computed and intermediate steps are required with simplifying assumptions. The following section explains three methodologies that can be used to choose a blade design for minimum cabin vibrations.

### 5.1.2.1. Methodologies available

Three methods are identified in the research and industrial roadmaps. All the three start from a blade internal structure derived from the specified blade planform:

1. Calculation of blade eigenmodes: the internal structure of the blade is adapted so that the eigenfrequencies of the blade do not match any rotor excitation frequency. This is the basis for low loads in the cabin, but tradeoffs are difficult to decide because transmissibility in the different directions is not computed. Those eigenfrequencies calculations are predictive and reliable thanks to advanced blade models, such as BAM [31], which includes coupled bending-torsion assumption, accounts for double swept planforms and also includes the double loads path approach for rigid rotor calculations. Tradeoffs between the modes are based on engineering judgment in case it is required. This approach is currently used in the industry;
2. Calculation of hub loads: The internal structure and the planform of the blade are adapted so that the dynamic hub loads are minimized in all three directions for the forces and moments. Tradeoffs between the eigenmodes are intrinsic but still the transmissibility between the hub loads and the cabin vibrations are not known. Engineering judgment is used for possible tradeoffs between the directions of the loads. Research shows that advanced aerodynamic models can improve the prediction of hub loads without the use of expensive CFD simulations [34]. This approach is identified as the future step for industrial applications.
3. Calculation of cabin vibrations: The internal structure and the planform of the blade are adapted so that the vibrations in the cabin are minimized. Tradeoffs between the loads directions are intrinsic and also depend on the cabin structure. The main shortcomings to the industrial use of such a methodology are the need for a predictive finite element model of the cabin up to 25-30Hz, as well as an accurate aerodynamic description. This approach still needs to be improved by further research activities.

In this work, the methodology based on the calculation of the eigenmodes was chosen to drive the selection of the blade internal structure.

### 5.1.2.2. Description of the methodology

Recent developments have been achieved within the frame of the CHALLENGE AeRothermoMEchanique (CHARME) project partially funded by DGAC in the blade eigenfrequencies positioning. We present here an application case. The strategy to tune the eigenmodes of a blade is based on the assumptions that the eigenfrequencies of the blade must be as far as possible from the rotor harmonics to avoid the loads to be transmitted from the blade to the rotor and to the cabin.

We note that for a helicopter blade the structural stiffness in the flapping direction ( $EI_F \approx 10^4 \text{N.m}^2$ ) is one or two orders of magnitude lower than stiffness in the lead-lag direction ( $EI_{ll} \approx 10^6 \text{N.m}^2$ ). This is due to the blade chord which is much larger than the airfoil thickness.

Given the large contribution of the centrifugal force to the flapping stiffness, changing the flapping eigenmode properties is complex. The only effective lever to modify the flapping mode properties remains the mass distribution,

which is directly linked to the centrifugal stiffness. An additional mass can either increase or decrease an eigenmodes frequency depending on its radial position:

- The centrifugal stiffness (and therefore the eigenfrequencies) increases linearly with the distance between the mass and the rotational center of the rotor. Hence the mass must be located near the blade tip to increase its eigenfrequencies;
- The generalized mass increases with the amplitude of the motion of the added mass. Therefore the blade eigenfrequencies will decrease when the mass is added on an anti-node.

The tuning of the modal frequencies is made in four following steps. Steps 1 and 2 are related to the modal tuning with mass boxes. Steps 3 and 4 are related to the modification of the structure to correctly tune the torsion and lead-lag mode frequencies:

- i. Modal shape calculation: this step aims at computing the blade modal shapes to identify the flapping modes which are not coupled with torsion, for which only the mass distribution can be used to modify the eigenfrequencies;
- ii. Mass box tuning: a sweeping analysis is made to choose the position of the mass box(es) that optimizes the flapping eigenfrequencies. In particular the position and the weight of the box is cautiously chosen.

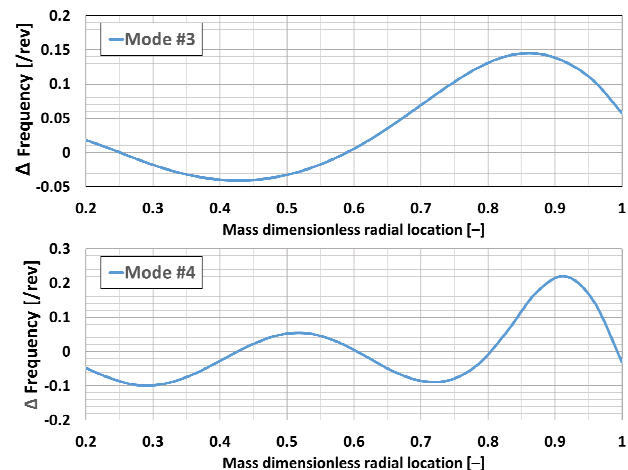


Figure 12 – Effect of the mass-box radial location on the distance to objective of some flapping-mode eigenfrequencies (fixed given mass)

For some applications, the mass is split into two boxes to respect integration and centering constraints. Figure 12 shows the eigenfrequencies of some flapping modes as a function of the mass-box radial location for a fixed mass;

- iii. Sensitivity analysis: this step is performed to reduce the number of degrees of freedom (as illustrated in Figure 13) in the design of experiments. Therefore, a sweeping analysis is made on each degree of freedom of the blade to check whether or not the parameter is relevant to tune the blade eigenfrequencies. Typical parameters are: the number of composite layers in the skin, the position of the torsion box and the number of composite layers in the trailing edge.

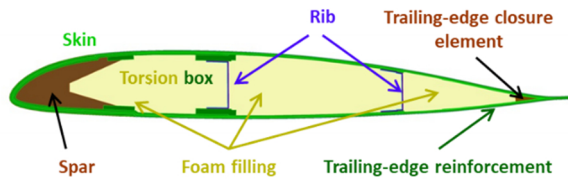


Figure 13 – Internal-structure degrees of freedom

- iv. Design of experiments: A full factorial Design of Experiments is performed to choose the best internal structure, which is the one for which the blade eigenfrequencies are the furthest from the rotor harmonics.

## 5.2. Modules inside the optimization loop

### 5.2.1. Selecting the fittest donor blade

For each candidate, donor blades are ranked as suitable donors based on the similarities in the chord and offset laws. Twist is considered to be transparent with regards to the structural properties. The spanwise integral squared difference between geometric laws (i.e. chord and offset) are the metrics used to determine the most suitable donor. A first set of donor blades is selected and sorted based on the chord-error metric. Best donors are extracted into a subset which is then ranked according to the offset-error metric.

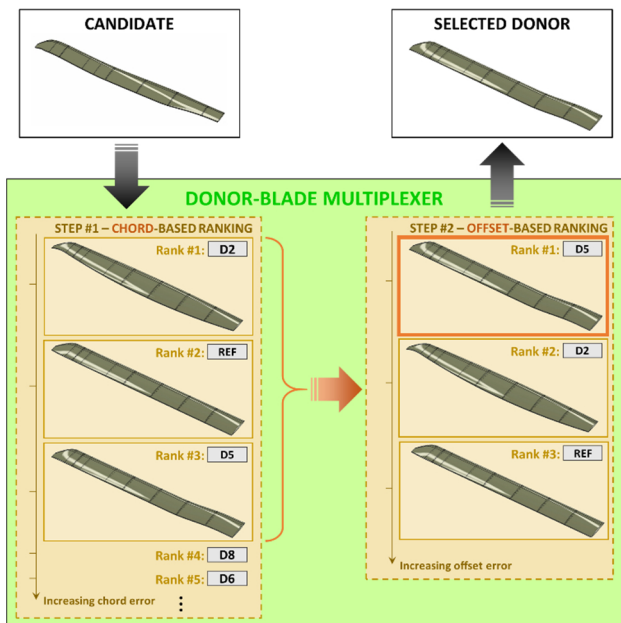


Figure 14 – Example of the selection of the fittest donor blade for a given random candidate

The selected donor blade is the blade ensuring the minimum deviation within this subset. The main idea behind this selection process is to use chord similarity as the main metric and offset as an auxiliary indicator when chord error values are similar. An example is given in Figure 14.

### 5.2.2. Adapting the candidate internal properties

We present in this section how the structural properties of blade candidates are now extrapolated from the selected donor blade. It has to be mentioned that a simple linear interpolation of the blade structural properties is not possible, since a homothetic transformation of the geometry

does not necessarily lead to a homothetic change of the internal structure, as depicted in Figure 15 (trailing edge reinforcement, spar area, similar skin- and-rib thickness)

The developed tool is based on laws that empirically determine the evolution of the elastic and inertial characteristics of blades following a geometric change. Those laws use geometric gradients to give the value of a parameter as a function of a prescribed blade which is expected to have close properties and similar technologies.

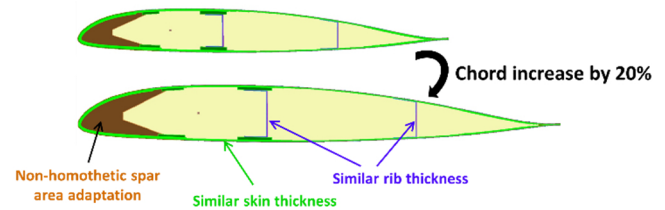


Figure 15 – Example of an homothetic chord change (20%) with an associated non-homothetic update of the internal structure

The exploration of blade planforms is made around a predefined donor blade. For each cross section, linear mass, mass inertia, center-of-gravity location as well as stiffnesses (tensile, flapping, drag, torsion) and principal inertia axes are updated with respect to a change of the chord, offset of the quarter-chord location, twist angle and airfoils. For a chord change, usual explorations do not exceed 10% of the donor value and thus the maximum chord change which is manageable by this low-fidelity tool is typically 20%. For example, at a given radial location  $r$ , the extrapolation law for a chord change is of the form:

$$(6) \quad X_{\text{candidate}}(r) = X_{\text{donor}}(r) \left( \frac{c_{\text{candidate}}(r)}{c_{\text{donor}}(r)} \right)^{\kappa_X}$$

where  $X$  is a placeholder for any elastic and inertial characteristics, and  $c$  is the chord. The subscripts refer either to the donor or to the considered candidate. The quantity  $\kappa_X$  is a parameter experimentally defined as a function of the airfoil relative thickness at the given radial location  $r$ .

For such laws to be valid, we assume that the geometrical changes of the blade planform are small enough and do not lead to any significant change of the blade modal properties with respect to the donor blade. This empirical method cannot take into account significant geometrical changes (such as the chord law) which modify the mass distribution. The addition of a tuning mass (chordwise or spanwise) or of composite layers are not within the scope of this tool.

## 6. RESULTS

An optimization process is launched including all the processing blocks previously introduced. The optimization is carried out using an initial seed of 400 individuals for 25 generations with a mutation probability of 10%. A rule of thumb was applied to size the population using roughly 10 individuals per parameter, for a total of around 200 individuals. A rate of 50% of rejection is expected in the pre-processing checks for the first generations (cf. section 4.5). This is why the population size is raised to 400 individuals. A second run continuing the previous optimization using 200 individuals including the former Pareto front for 60 additional generations is subsequently carried out so as to fully converge and populate the Pareto Front.

The candidate rejection rates — either because the geometric coherence check failed or because the simulation did not converge — are presented in Figure 16 for the two runs. The number of discarded candidates diminishes rapidly after the first generation and the re-used-candidate rate increases as the Pareto Front is populated. The reason why the second run — based on a restart using the Pareto Front of the previous one — shows discarded candidates is that the Pareto Front of the first run was constituted of less than 200 individuals. Thus, the generation of additional candidates was needed to entirely populate the starting generation of the second run.

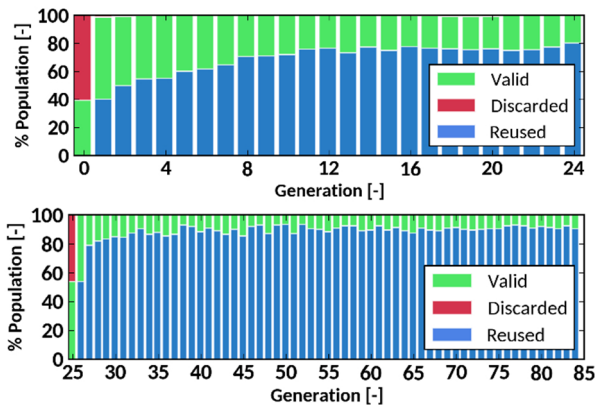


**Figure 16 – Rate history of valid-candidate production, discarded candidates and re-used candidates from previous generations; top: first optimization using 400 individuals (run #1), bottom: restart using 200 individuals (run #2)**

### 6.1. Pareto optimal front

The Pareto front obtained at the end of the optimization process is presented in Figure 17. The reference blade corresponds to the straight donor blade. Acceptable thresholds values for each function are represented as green lines according to the objectives presented in Section 3. The green zone thus highlights all the candidates which comply with the fixed objectives.

The maximum expected gains in hover required power with respect to the baseline are of an order of magnitude lesser than the reductions of the pitch-link dynamic loads that can be obtained in high-speed flight.

The Pareto front presents a discontinuity in the highlighted zone. This can be an indication that the optimizer found two local optima located in separated regions of the design space, to be confirmed by the analysis of the Pareto optimal design parameters.

### 6.2. Design robustness

The design parameters corresponding to Pareto optimal candidates are shown in Figure 19. For the sake of clarity, Bézier inner points of the chord and offset laws (which control the geometric law tangencies) are not included, as their physical interpretation is not straightforward.

Each parameter has been normalized with respect to its mathematical space-design boundaries so that 0 and 1 correspond respectively to the lower and upper limits. The parameters are represented as a function of the Pareto-front spread, which is the result of parameterizing the Pareto front by its arc-length in a normalized objective space (i.e. zero value starting at the asymptotic hover optimum and up to 1 for the asymptotic loads optimum).

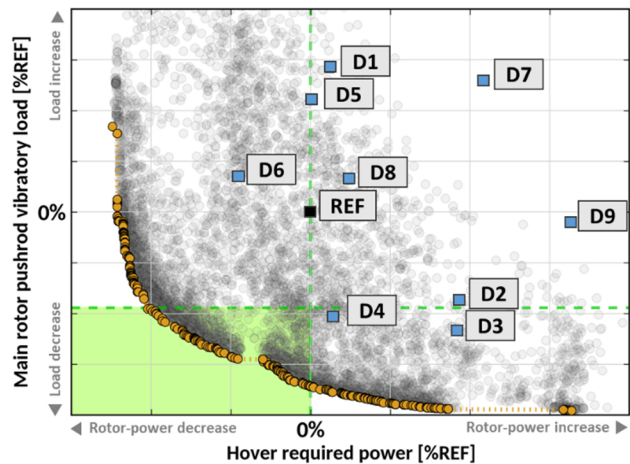


**Figure 17 – Converged Pareto Front (in orange); donor blade designs (D<sub>i</sub> in blue) and all computed candidates (in grey). The objective targeted area is highlighted in green**

This representation allows an effective visualization of all the Pareto optimal designs. A gap splitting the Pareto front into two main blade families can be observed, confirming the hypothesis of two local optima. It is also demonstrated that inside a given Pareto family, the parameter scattering is rather small. As a consequence, nearby Pareto optimal designs correspond to nearby candidates in the design space.

The hover-optima family favours large negative twist rates in the inner-blade region as well as in the tip region with opposed trends for the loads objective. The twist rate within the spanwise range  $[0.7R, 0.9R]$  is saturated to the maximum allowed boundary through the whole Pareto Front, as a result of mitigating aeroelastic phenomena in the advancing side.

Loads optima show chord distributions with a reduced chord at the blade-root region with strong taper, while hover optima favour opposite trends, with chord reductions in the outer sections of the blade. Concerning offset laws, loads optima demonstrate a V-shaped law with forward offsets with respect to the pitch axis in the blade-root and tip region along with a backward offset around  $0.6R$ . On the other hand, hover optima follow opposite trends. This illustrates the antagonism between the objectives in hover and high-speed cruise.

A compromise candidate (referred to as OPT in the following sections) was chosen in order to retain the same expected hover performance of the reference straight blade while minimizing dynamic pitch-link loads at high speed, thus fulfilling the objectives presented in section 3. The OPT blade planform is shown in Figure 18.

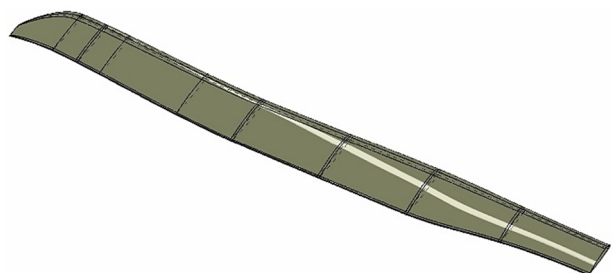


**Figure 18 – Selected candidate at iso-required power w.r.t. reference straight blade and minimizing dynamic loads in high-speed forward flight (OPT)**

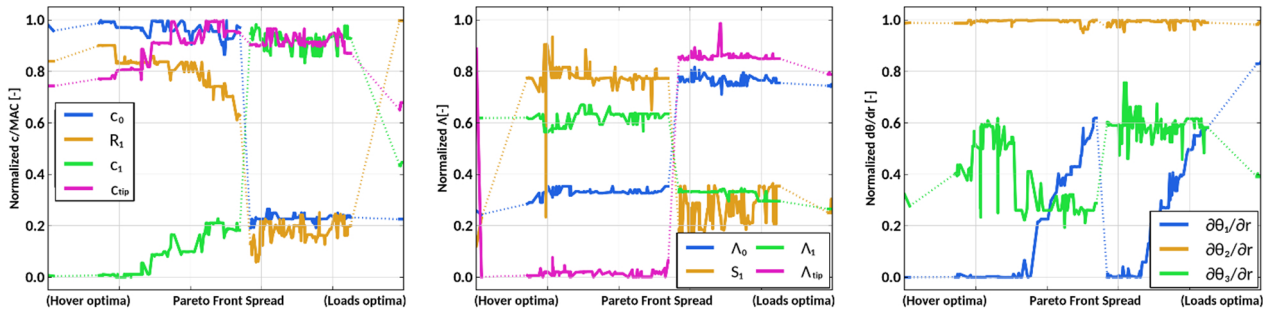


Figure 19 – Pareto optimal design variables controlling the chord (left), offset (middle) and aerodynamic twist (right) laws. Variable values are normalized by their boundaries and ordered following the Pareto Front curve

## 7. SOLUTION CONSOLIDATION

The OPT candidate extracted from the Pareto Front has to be consolidated with regards to each of the simplifying hypotheses made throughout the simulation workflow. As a first step the fidelity of the aerodynamic simulations and the accuracy of the automated tool updating the structural properties are evaluated independently.

### 7.1. Internal structural properties

The methodology described in 5.1.2.2 is used to tune the blade structural properties of the OPT candidate in order to comply with eigenmodes, stability and inertial criteria.

The initial hypothesis considered that the mass box distribution of the new candidates would remain close to the donor's one. Thus the flapping eigenmodes should remain close to the donor's modes. The eigenmode frequencies for the automated structural properties are compared in Figure 20 with the eigenfrequencies of the original donor blade and the tailored blade with respect to a common objective.

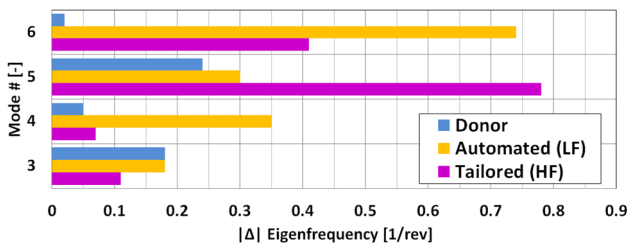


Figure 20 – Distance to the objective eigenfrequencies for the blade with automatically updated structural properties and the tailored version

The first elastic mode (#3, 2<sup>nd</sup> flapping mode) remains close for all blades. However, important differences can be observed for modes #4 (2<sup>nd</sup> lead-lag mode), #5 (1<sup>st</sup> torsion mode) and #6 (3<sup>rd</sup> flapping mode).

The changes in the flapping-mode frequencies can be in part explained by the fact that the mass box of the OPT candidate must be significantly displaced with respect to its position in the donor blade. Additionally, lead-lag sectional rigidity must be augmented in order to reduce the eigenfrequency of the 4<sup>th</sup> mode.

### 7.2. Dynamic loads

Due to the high computational cost associated with forward flight computations, CFD is not used to evaluate the helicopter dynamic loads in forward flight. It is evident that the inclusion of higher-fidelity aero elastic simulations is mandatory to correctly capture the aerodynamic phenomena and the 3D effects. However, given the scope of this work, we choose to evaluate only the impact of the structural updates for a given aerodynamic model. The aerodynamic model remains consequently the same as in the optimization simulations and the dynamic loads are re-evaluated taking into account just the tailored blade structural properties instead of the automated ones.

The results are presented in Figure 21. The discrepancies in dynamic loads between the automatically updated blade (OPT LF, i.e. Low-Fidelity) and the tailored one (OPT HF, i.e. High Fidelity) can be read on the y-axis. Even if the loads significantly increase after taking into account the higher-fidelity structural definition the candidate remains below the loads objective threshold. This degradation can be explained by the fact that dynamic loads are significantly affected by the aero elastic response of the blade. Thus, as expected, the change in the eigenmodes placement (and incidentally in the centering of the resulting blade) has a non-negligible impact on the dynamic loads.

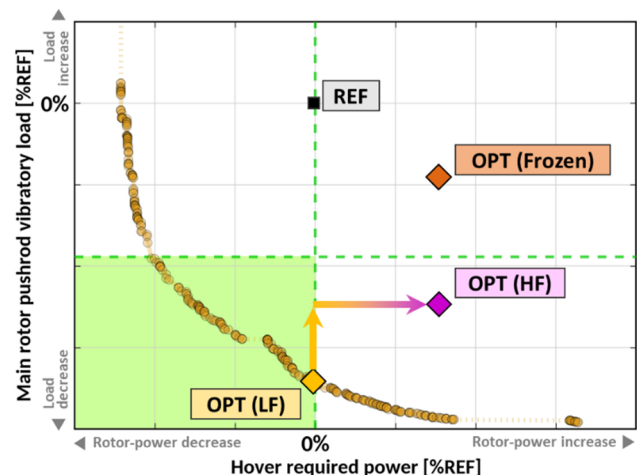


Figure 21 – Update candidate OPT (HF) evaluated with CFD in hover and tailored structural properties in forward flight (Nota: the rest of the Pareto Front is not recomputed with higher-fidelity tools)

However, it should be noted that even if the automatic structural update is not yet perfectly tuned, it is still better than considering no update at all. Indeed, the OPT candidate has also been recomputed using frozen structural properties, namely those of the reference blade (REF). This candidate (OPT Frozen in Figure 21) is still better than the reference with respect to the dynamic loads, but the gains are significantly diminished with respect to the OPT HF candidate. This reduction could be explained by the fact that aerodynamics are improved. If aerodynamics were the sole responsible this would indicate that 38% of the gains of OPT HF can be attributed to aerodynamics and 62% to the structural response of the blade. Unfortunately, the dynamic loads reduction is a coupled aero elastic problem and thus it is not as straightforward to discriminate the sources of the benefits.

### 7.3. Performance

The performance analysis requires taking into account the exhaustiveness of the external conditions. To this goal, the full rotor polar has been computed by CFD for the reference blade and the OPT HF candidate. An air density/RPM reduction has been considered to guarantee that the hover domain is fully covered.

The elsA CFD code [6] developed at ONERA was used. The code solves the compressible 3-D RANS equations using a cell centered finite-volume method. The turbulence is modeled using the Menter  $k - \omega$  model with the shear stress transport (SST) correction. The flux is discretized using Jameson's scheme. The time integration is performed using an implicit algorithm based on a backward Euler scheme.

A fraction of an isolated rotor comprising a single blade was simulated using a Chimera assembly with a near-body grid immersed in a background octree mesh (i.e. a cylinder fraction) using periodic boundaries and imposing sink-hole Froude conditions, as illustrated in Figure 22. The blade was considered rigid and no coupling with HOST was performed.

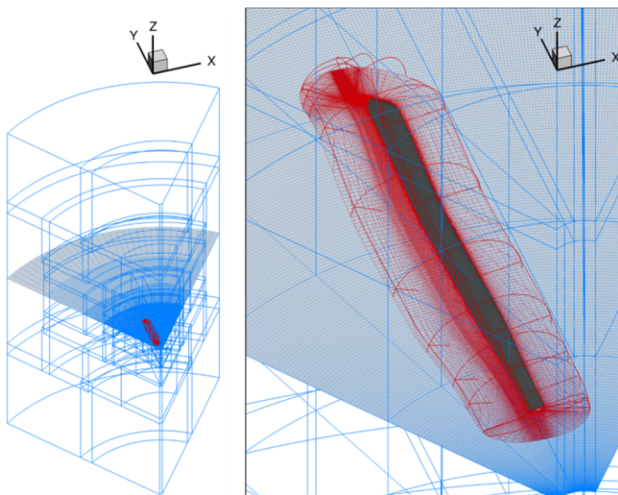


Figure 22 – Overview of the Chimera assembly; Near-body grid in red, background octree grid in blue

Complete rotor polars were thus obtained by varying the collective-pitch angle, as shown in Figure 23. The results were compared at same thrust and the differences between the HOST simulations and the CFD results can be read in the x-axis in Figure 21. The higher-fidelity results present a

very slight penalty of the hover efficiency at the objective thrust. This underlines the importance of the 3D effects in the hover evaluation especially in the blade tip region. Nevertheless, first order effects such as the blade twist law are correctly captured. It should be noted that the gains in hover required power illustrated in the Pareto Front are an order of magnitude lower than the reductions in dynamic loads with respect to the reference blade. In addition, the significant load improvement from the OPT candidate paves the way for mass-reduction loops of some rotor components, thus potentially offsetting the slight hover performance degradation.

The error between the low and high fidelity evaluations of the required power in hover remains inferior to 1% with respect to the reference.

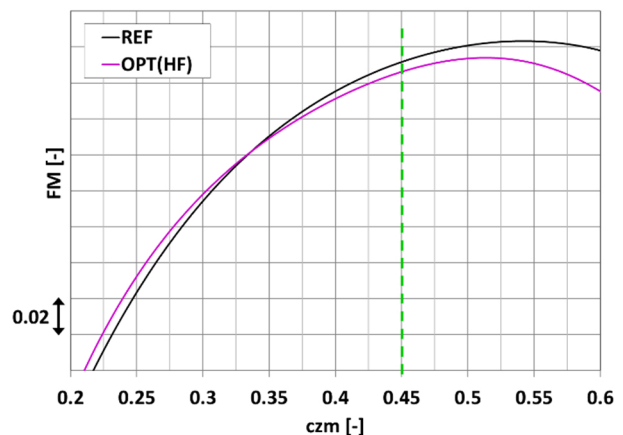


Figure 23 – Figure of Merit with respect to the mean blade loading coefficient for the reference blade (REF) and the optimization candidate (OPT HF); The mean blade loading at which the blades are compared is depicted in green

These computations were subsequently used in order to perform more in-depth performance analysis following the guidelines presented in Section 3.2.

## 8. CONCLUSIONS

This study presents recent optimization work performed at Airbus Helicopters in the framework of the RAPACE project. The main topic concerns the automatic adaptation of the structural properties of a rotor blade when performing blade platform optimizations. These include design variables such as twist, chord and offset radial laws.

The update of the structural properties was achieved by comparing each blade candidate to a pool of potential tailored donors, selecting the most appropriate one based on geometric similarity and extrapolating the structural sectional characteristics based on semi-empirical laws. The underlying assumption being that the resulting extrapolated blade should present acceptable modal properties as well as appropriate stability (eigenfrequencies tuning, stability criteria).

This capability was integrated in a fully automated multi-objective optimization workflow relying on fast evaluation methods in order to explore potential candidates. The design objectives included the minimization of required power in hover as well as the reduction of main rotor pushrod dynamic loads in high-speed cruise. An interesting candidate among the resulting Pareto-optimal solutions was selected, preserving the same required power in hover

as a straight reference blade while reducing the dynamics pushrod loads in forward flight.

This candidate was then recomputed using higher fidelity tools. In hover, CFD was used considering a rigid blade and an isolated rotor. The resulting differences of low and high fidelity simulations with respect to the baseline blade were less than 1%. However the differences highlight the importance of 3D effects, which should be taken into account for higher accuracy of the predictions. In forward flight, the aerodynamic model was not upgraded (no free wake simulations or CFD coupling were implemented). Only the effect of the structural properties update was analyzed. The results show that albeit the sectional structural properties of the automated candidate are acceptable, additional efforts are required to ensure that the blade eigenfrequencies are correctly tailored. The hypothesis assuming that the donor blade and the candidate blade would have very similar eigenmodes was not entirely verified. The spanwise placement of the tuning mass box had a significant effect on the flapping modes that had to be corrected a posteriori. Nevertheless, the inclusion of the automatic structural update was demonstrated to be beneficial.

The presented method shows very promising results and demonstrates its usefulness in an industrial context. Going forward, mode-frequency tailoring can be integrated as a nested optimization for each candidate and structural properties can be directly used as design variables for the load reduction problem.

## ACKNOWLEDGEMENTS

This work was supported by the Rotor hAutes PerformAnCes urbainEs (RAPACE) and CHALLENGE AeRo-thermo-MEchanique (CHARME) Projects, partially funded by Direction Générale de l'Aviation Civile (DGAC). The authors are grateful for the support from Jean-Romain Bihel, Jean-François Hirsch, Paul Cranga, Paul Eglin, Manousos Kelaidis, Guillaume Depommier, Guillaume Legras & David Alfano.

## COPYRIGHT STATEMENTS

The authors confirm that they, and/or their company or organization, hold copyright on all of the original material included in this paper. The authors also confirm that they have obtained permission, from the copyright holder of any third party material included in this paper, to publish it as part of their paper. The authors confirm that they give permission, or have obtained permission from the copyright holder of this paper, for the publication and distribution of this paper as part of the ERF proceedings or as individual offprints from the proceedings and for inclusion in a freely accessible web-based repository.

## ABBREVIATIONS

BET	Blade Element Theory
CAD	Computer-Aided Design
CFD	Computational Fluid Dynamics
CSD	Computational Structural Dynamics
CHARME	Challenge AeRoMEchanique
DGAC	Direction Générale de l'Aviation Civile
FISUW	Finite State Unsteady Wake model
HEMS	Health & Emergency Medical Services

H <sup>3</sup>	High-speed Hybrid Helicopter
HOST	Helicopter Overall Simulation Tool
ISA	International Standard Atmosphere
MOGA	Multi-Objective Genetic Algorithm
NSGA	Non-dominated Sorting Genetic Algorithm
RACER	RApid and Cost-Effective Rotorcraft
RAPACE	Rotor hAutes PerformAnCes urbainEs
RSRA	NASA Rotor Systems Research Aircraft
SAR	Search and Rescue
SL	Sea Level
X <sup>3</sup>	eXperimental High-speed Hybrid Helicopter

## SYMBOLS

AoA	Angle of attack	[deg]
$c(r)$	Chord law	[m]
$c_{zm}$	Blade loading coefficient $c_{zm} = \frac{6T}{5\rho MAC \Omega^2 R^3}$	[-]
$EI$	Structural stiffness	[Nm <sup>2</sup> ]
FM	Figure of Merit	[-]
MAC	Mean aerodynamic chord	[m]
$r$	Radial position along the blade	[m]
$R$	Main-rotor radius	[m]
$R_0$	First airfoil station location	[m]
$R_{tip}$	Start location of the blade-tip region	[m]
$T$	Rotor thrust	[N]
$U$	Rotorcraft translation speed (cruise)	[m/s]
$\theta(r)$	Twist law	[deg]
$\Lambda(r)$	Offset law	[-]
$\mu$	Advance ratio: $\mu = \frac{U}{\Omega R}$	[-]
$\rho$	Air density	[kg/m <sup>3</sup> ]
$\Omega$	Main-rotor angular velocity	[rad/s]

## REFERENCES

- [1] **Airbus Helicopters**, *Airbus Helicopters reveals RACER high-speed demonstrator configuration*, <https://www.airbus.com/newsroom/press-releases/fr/2017/06/Airbus-Helicopters-reveals-Racer-high-speed-demonstrator-configuration.html>, press release (2017)
- [2] **Arcidiacono, P.J., De Simone, G. & Occhiato, J.** *Preliminary evaluation of RSRA data comparing pure helicopter, Auxiliary propulsion and Compound helicopter flight characteristics*, American Helicopter Society 36, Washington D.C., USA (1980).
- [3] **Bailly, J., Ortun, B., Delrieux, Y., Mercier & Des Rochettes, H.**, *Recent Advances in Rotor Aerodynamic Optimization, Including Structural Data Update*, Journal of the American Helicopter Society, Volume 62, Number 2, pp. 1-11(11) (2017).
- [4] **Bailly, J. & Bailly, D.**, *Multi-Fidelity Aerodynamic Optimization of a Helicopter Rotor Blade*, AIAA Journal, pp. 1-2, (2019).
- [5] **Benoit, B., Dequin, A.M. & Kampa, K., VonGrünhagen W., Basser P.M. & Gimonet, B.**, *HOST, a general helicopter simulation tool for Germany and France*, 56<sup>th</sup> Annual Forum of the American Helicopter Society, Virginia Beach, USA (2000).

- [6] **Cambier, L., Heib, S., & Plot, S.**, *The Onera elsA CFD software: input from research and feedback from industry*, Mechanics & Industry, Vol. 14, 2013, pp. 159-174.
- [7] **Choi, S., Potsdam, M., Lee, K. Iaccarino, G. & Alonso, J. J.**, *Helicopter Rotor Design Using a Time-Spectral and Adjoint-Based Method*, Journal of Aircraft, Volume 51, Number 2, pp. 412-423, (2014).
- [8] **Collins, K. B., Sankar, L. N. & Mavris, D. N.**, *Application of low-and high-fidelity simulation tools to helicopter rotor blade optimization*, Journal of the American Helicopter Society Volume 58, Number 4, October 2013, pp. 1-10(10).
- [9] **Deb, K., Pratap, A., Agarwal, S. & Meyarivan, T.**, A fast and elitist multiobjective genetic algorithm: NSGA-II, IEEE transactions on evolutionary computation, 6(2), p. 182-197 (2002).
- [10] **Dumont, A., Le Pape, A., Peter, J. & Huberson, S.**, *Aerodynamic shape optimization of hovering rotors using a discrete adjoint of the Reynolds-Averaged Navier–Stokes Equations*, Journal of the American Helicopter Society, Volume 56, Number 3, pp. 1-11. (2011).
- [11] **Ganguli, R.**, *Survey of Recent Developments in Rotorcraft Design Optimization*, Journal of Aircraft 41(3), pp. 493-510 (2016).
- [12] **Ganguli, R., & Chopra, I.**, *Aeroelastic optimization of a helicopter rotor with two-cell composite blades*, AIAA Applied Journal, 34(4), pp. 835-841 (1996).
- [13] **Glaz, B., Friedmann, P. P. & Liu, L.**, *Surrogate based optimization of helicopter rotor blades for vibration reduction in forward flight*, Structural and Multidisciplinary Optimization, 35 no 4, pp. 341-363. (2008).
- [14] **Goldberg, D.**, *Genetic algorithms in search, optimization and machine learning*, 1<sup>st</sup> ed. Addison-Wesley Longman Publishing Co. Inc., Boston, USA (1989).
- [15] **Hirsch, J.F., Alfano, D., Cranga, P., Gareton, V. & Guntzer, F.** *The Blue Edge™ Blade Continuation*, VFS 75<sup>th</sup> Annual Forum & Technology Display, Philadelphia PA, USA (2019).
- [16] **Imiela, M. & Wilke, G.**, *Passive Blade Optimization and Evaluation in Off-Design Conditions*, 39<sup>th</sup> European Rotorcraft Forum, Moscow, Russia (2013).
- [17] **Imiela, M.**, *High-fidelity optimization framework for helicopter rotors*, Aerospace Science and Technology, 23(1), pp. 2-16 (2012).
- [18] **Leishman, J.G.**, *Principles of helicopter aerodynamics*, 2<sup>nd</sup> edition, Cambridge aerospace series (2016).
- [19] **Lentine, F.P. Groth, W.P. & Oglesby, T.H.** *Research in Maneuverability of the XH-51A Compound helicopter*, ASAAVLABS Technical Report 68.2 (1968).
- [20] **Leusink, D., Alfano, D. & Cinnella, P.**, *Multi-fidelity optimization strategy for the industrial aerodynamic design of helicopter rotor blades*, Aero. Sci. Tech., 42, pp.136-147 (2018).
- [21] **Lim, J. W.**, *Consideration of structural constraints in passive rotor blade design for improved performance*, The Aeronautical Journal 120 no 1232, pp 1604-1631 (2016).
- [22] **Mishra, A., Mani, K., Mavriplis, D. J., & Sitaraman, J.**, *Helicopter rotor design using adjoint-based optimization in a coupled CFD-CSD framework*, In 31<sup>st</sup> AIAA Applied Aerodynamics Conference, pp. 2906 (2013).
- [23] **Öhrle, C., Frey, F., Thiemeier, J., Keßler, M., Krämer, E., Embacher, M., Cranga, P. & Eglin, P.**, *Compound helicopter X3 in high-speed flight: correlation of simulation and flight tests*, Vertical Flight Society Forum 75, Philadelphia, USA (2019).
- [24] **Orchard, M.N. & Newman, S.J.** *The compound helicopter – Why have we not succeeded before?*, The Aeronautical Journal, 103, p.489-495 (1999).
- [25] **Ormiston, R. & Basset, P.M.**, *Comparison and validation of the France/US finite state rotor dynamic inflow models*, 36<sup>th</sup> European Rotorcraft Forum, Paris, France (2010).
- [26] **Paris, M.**, *Torsionnal behavior identification of a conventional helicopter blade and rotor at high advance ratio : application to the reduction of control loads on the X3-type hybrid helicopter*, Ph.D. thesis, Ecole Nationale Supérieure des Arts et Métiers de Paris (2014).
- [27] **Pözlbauer, P., Desvigne, D. & Breitsamter, C.**, *Aerodynamic design optimization of a helicopter rotor blade-sleeve fairing*, CEAS Aeronaut. J. (2018).
- [28] **Roca León, E., Le Pape, A., Désidéri, J. A., & Alfano, D.**, *Multi-Fidelity Concurrent Aerodynamic Optimization of Rotor Blades in Hover and Forward Flight*, 40<sup>th</sup> European Rotorcraft Forum, Southampton, UK (2014).
- [29] **Roca León, E., Le Pape, A., Costes, M., Désidéri, J. A., & Alfano, D.**, *Concurrent Aerodynamic Optimization of Rotor Blades Using a Nash Game Method*, Journal of the American Helicopter Society, Volume 61, Number 2, pp. 1-13 (13) (2016).
- [30] **Segel, R., Jenney, D. & Gerdes, W.** *Final report of the NH-3A (Sikorsky S-61F) flight test program*. Sikorsky Aircraft Corporation, Tech. Rep. SER 611344 (1969).
- [31] **Skladanek, Y., Cranga, P., Ferraris, G., Jacquet, G. & Dufour, R.**, *A non-linear Beam Finite Element for curved and twisted composite helicopter blade*, 36<sup>th</sup> European Rotorcraft Forum, Paris, France (2010).
- [32] **Stanger, C., Hollands, M., Keßler, M. & Krämer, E.**, *Adaptation of the Dynamic Rotor Blade Modelling in CAMRAD for Fluid-Structure Coupling Within a Blade Design Process*, New Results in Numerical and Experimental Fluid Mechanics IX, pp. 263-271 (2014).
- [33] **Vuillet, A., Allongue, M. Philippe, J.J. & Desopper, A.** *Performance and aerodynamic development of the Super Puma Mk2 main rotor with new SPP8 blade tip design*, 15<sup>th</sup> congrès sur les hélicoptères, ONERA TP n° 1989-181 (1989).
- [34] **Wilke, G.**, *Applying Multi-Objective Variable-Fidelity Optimization Techniques to Industrial Scale Rotors: Blade Designs for CleanSky*, 41<sup>th</sup> European Rotorcraft Forum, Munich, Germany (2015)